

Quantum Hall phase emerging in an array of atoms interacting with photons

Alexander V. Poshakinskiy,¹ Janet Zhong,² Yongguan Ke,^{2,3} Nikita A. Olekhno,⁴
Chaohong Lee,^{3,5} Yuri S. Kivshar,^{2,4,*} and Alexander N. Poddubny^{1,2,4,†}

¹*Ioffe Institute, St. Petersburg 194021, Russia*

²*Nonlinear Physics Centre, Australian National University, Canberra ACT 2601, Australia*

³*Guangdong Provincial Key Laboratory of Quantum Metrology and Sensing & School of Physics and Astronomy,
Sun Yat-Sen University (Zhuhai Campus), Zhuhai 519082, China*

⁴*ITMO University, St. Petersburg 197101, Russia*

⁵*State Key Laboratory of Optoelectronic Materials and Technologies,
Sun Yat-Sen University (Guangzhou Campus), Guangzhou 510275, China*

(Dated: March 19, 2020)

Topological quantum phases underpin many concepts of modern physics. While the existence of disorder-immune topological edge states of electrons usually requires magnetic fields, direct effects of magnetic field on light are very weak. As a result, demonstrations of topological states of photons employ synthetic fields engineered in special complex structures or external time-dependent modulations. Here, we reveal that the quantum Hall phase with topological edge states, spectral Landau levels and Hofstadter butterfly can emerge in a simple quantum system, where topological order arises solely from interactions without any fine-tuning. Such systems, arrays of two-level atoms (qubits) coupled to light being described by the classical Dicke model, have recently been realized in experiments with cold atoms and superconducting qubits. We believe that our finding will open new horizons in several disciplines including quantum physics, many-body physics, and nonlinear topological photonics, and it will set an important reference point for experiments on qubit arrays and quantum simulators.

The study of electrons propagating in magnetic fields has been driving many problems of physics since the discoveries of the Landau levels [1] and a self-similar structure of the energy spectrum in crystals subjected to ultrahigh magnetic fields [2, 3]. Quantum Hall effect [4] and topological insulators [5, 6] brought the concepts of topological phases to condensed matter physics. However, many effects predicted long time ago including the Hofstadter butterfly spectrum have been realized only recently [7].

These developments inspired a rapid progress in *topological photonics* aiming at creating robust edge states of light immune to disorder [8–11]. Since the effects of magnetic fields on light are weak, the realisation of topological concepts in photonics requires artificial structures and metamaterials [12]. Alternative approaches rely on time modulation of structure parameters [13–16] or engineered nonlinearities [17, 18]. These approaches allow creating effective gauge fields in real or synthetic dimensions, and mimic the effects of magnetic fields or spin-orbit couplings for photons.

Here, we uncover that the hallmarks of the quantum Hall phases, including Landau energy levels, topological edge states, and Hofstadter butterfly spectrum, can appear in a simple quantum system: an array of closely spaced two-level atoms (qubits) coupled to photons in a waveguide, see Fig. 1a. In this system, photons become strongly coupled to atoms and create *polaritons*. These polaritons are not independent but strongly interacting, because one atom cannot absorb two photons simultaneously [21]. While the considered model is paradigmatic for quantum optics [22–24], its two-particle Hilbert space

was not analyzed until recently. As shown in Figs. 1(c,d), when the polariton wave vector is comparable with that of light, a collective atomic state is easily excited optically, and it generally gets “darker” for larger wave vectors. In a two-particle “bright” state, the wave vectors of both excitations are small, which corresponds to the Dicke superradiance [25]. Novel two-particle dark states, where both wave vectors are large, were predicted only last year, and they originate from fermionization of strongly interacting polaritons [26]. It has also been suggested that interactions in the corner regions [19] of the diagram of Fig. 1d can localize one of the two polaritons in the center of the array [20].

In this paper, we predict novel types of topological edge states driven by polariton-polariton interactions in the regions indicated by butterflies in Fig. 1d. Here, one polariton forms a standing wave with multiple nodes and a periodic potential for the other indistinguishable polariton, see Figs. 1(b,e). As a result, the interaction is described by the *self-induced* Aubry-André-Harper [27] model that is mathematically equivalent to the quantum Hall problem on a lattice [28, 29].

The striking novelty of our prediction is that the quantum Hall phase can emerge for interacting indistinguishable particles without any special fine-tuning. The periodic modulation is an intrinsic feature that arises naturally due to the polariton-polariton interactions, in a sharp contrast to previous studies [30, 31], where one had to impose the modulation deliberately, either by engineering the lattice [31, 32] or applying external fields [11, 15]. The full Hofstadter butterfly-like spectrum could be obtained in a single shot from just one fixed

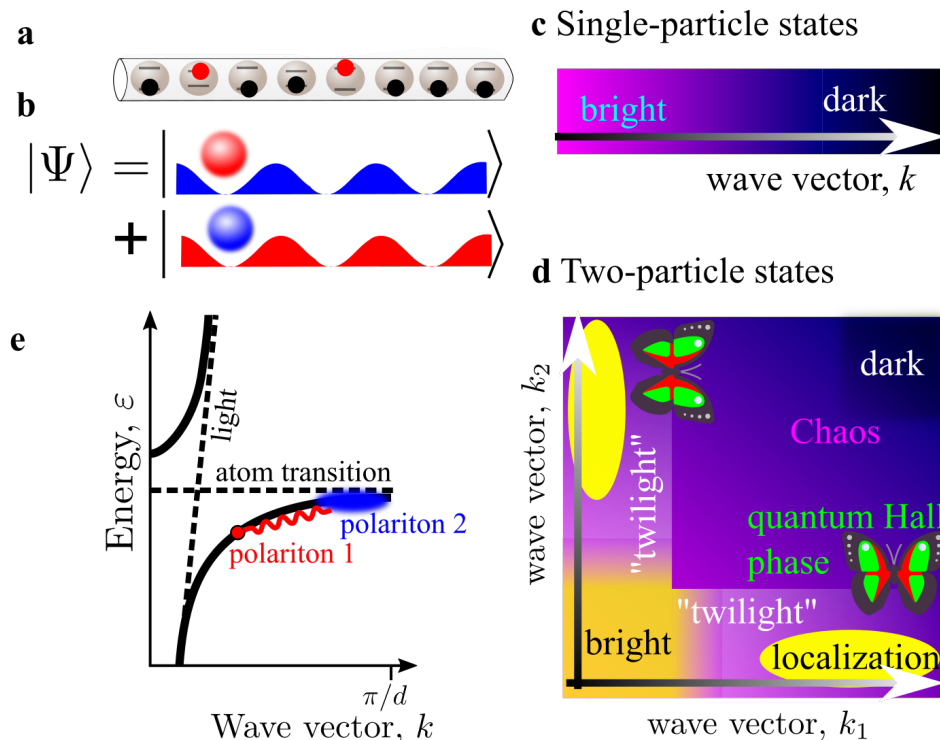


FIG. 1. **Emergence of quantum phases due to polariton-polariton interaction.** (a) Double-excited array of two-level atoms (qubits) in a waveguide. (b) Two-polariton quantum states where each indistinguishable polariton induces a potential for the other one. (c) and (d): Classification of single- and double-excited states of the atomic array depending on the wave vector of the excitations. Butterflies in (d) indicate the regions where the quantum Hall phase and Hofstadter-like butterfly spectrum emerge from the interaction of two excitations. Regions of “twilight” states [19] and interaction-induced localization [20] are also shown. (e) Single-particle polaritonic dispersion. Interaction of a lower-branch polariton with small k and that with large k is illustrated.

atomic array, eliminating the need to continuously tune an external magnetic field in a conventional setup [7, 15]. Our results apply to the experiments with cold atoms [33] or superconducting qubits coupled to a waveguide [34–40] and emerging quantum simulators based on excitonic polaritons [41]. This offers new possibilities to understand quantum many-body topological phases of interacting matter and protect them against decoherence.

TWO-POLARITON STATES

We consider a periodic array of two-level atoms (qubits) coupled to light, described by an effective Dicke-type Hamiltonian [19, 26, 42]

$$H = \sum_n \omega_0 \sigma_n^\dagger \sigma_n - i\Gamma_0 \sum_{n,m} e^{i\omega_0 d|n-m|/c} \sigma_n^\dagger \sigma_m, \quad (1)$$

where σ_n^\dagger is the operator creating excitation of the atom n with the resonance frequency ω_0 , $(\sigma_n^\dagger)^2 = 0$ and Γ_0 is the radiative decay rate of a single atom. While for $d = 0$ the Hamiltonian (1) is equivalent to the conventional Dicke model [25], even small interatomic spacings $0 < d \ll 2\pi c/\omega_0$ make the model considerably richer.

Single-particle eigenstates of Eq. (1) are polaritons with the energy dispersion $\varepsilon(k) = \omega_0 + \Gamma_0/[\cos kd - \cos(\omega_0 d/c)]$ [42, 43], schematically shown in Fig. 1e. The dispersion consists of two polaritonic branches, resulting from the avoided crossing of light with the atomic resonance and we focus on the lower branch. In the finite array of N atoms, the wave vectors are quantized $k_j d = \pi j/N$, $j = 1, 2, \dots, N$ [44], and the eigenstates are standing waves, see Figs. 2a–d. Negative imaginary part of the energies in Fig. 2a characterizes radiative decay into the waveguide. Crucially, the spectrum in Figs. 2a condenses near the resonance $\varepsilon = \omega_0$, where the group velocity of polaritons decreases.

Next, we proceed to the double-excited states $\Psi = \sum_{n,m} \psi_{nm} \sigma_n^\dagger \sigma_m^\dagger |0\rangle$. Their spectrum, obtained from the Schrödinger equation $H\Psi = 2\varepsilon\Psi$, is shown in Figs. 2e–h in different energy scales and demonstrates a distinct clustered structure. Each cluster resembles the single-particle spectrum in Fig. 2a and is formed by a polariton with a certain wave vector k_j interacting with polaritons with larger wave vectors. Therefore, most of the spectrum in Figs. 2e–g could be described by $\varepsilon \approx (\varepsilon_j + \varepsilon_i)/2$, where ε_j and ε_i are the single-particle energies from Fig. 2a. However, the dense part of the cluster, which

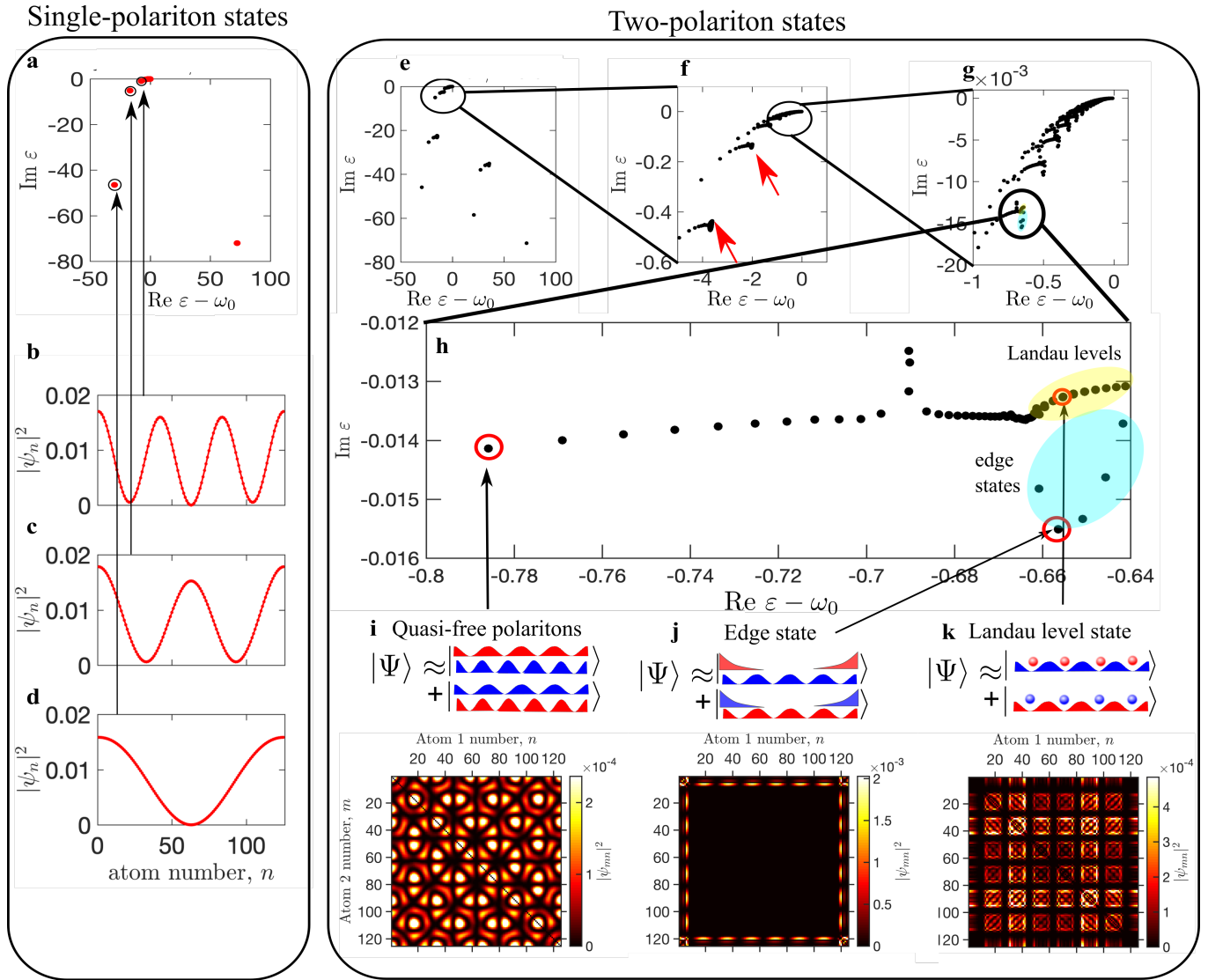


FIG. 2. **Single- and two-polariton energy spectra.** (a): complex energy spectrum of single-polariton modes. Three characteristic eigenstates are shown in panels b–d. (e–h): Two-polariton energy spectrum zoomed in different scales. (i,j,k): Spatial color maps of different characteristic two-polariton eigenstates $|\psi_{nm}|^2$. Calculation has been performed for $N = 125$ atoms and $\omega_0 d/c = 0.02$. Energy is measured in units of Γ_0 .

corresponds to $\epsilon_i \rightarrow \omega_0$ (see red arrows in Fig. 2f), is drastically transformed by the interaction. Three characteristic states from the cluster with $j = 7$ are presented in Figs. 2i–k. While the state in Fig. 2i is just a symmetrized product of two standing waves, weakly modified by interaction, the role of the interaction dramatically increases for $\text{Re } \epsilon - \omega_0 > -0.66\Gamma_0$ in Fig. 2h. The spectrum is split by interaction into relatively delocalized states with smaller radiative decay rate (yellow ellipse in Fig. 2h and Fig. 2k) and the states with larger radiative losses, where one of the two polaritons is localized at the edge of the structure (blue ellipse in Fig. 2h and Fig. 2j).

This interaction-induced transformation of the two-polariton spectrum is our central result. The delocalized states are almost $(j - 1)$ -fold degenerate, where j is the

cluster number and correspond to the Landau levels in the effective magnetic field. The states in Fig. 2j come in degenerate pairs corresponding to topological edge states localized at the opposite sides of the array.

LANDAU LEVELS, TOPOLOGICAL EDGE STATES, AND HOFSTADTER BUTTERFLY

We now present an analytical model explaining the topological origin behind the interaction-induced edge states in Fig. 2j. In the basis $|x\rangle = \frac{1}{\sqrt{N}} \sum_{n=1}^N \exp(i\omega_0 d|x-n|/c) \sigma_n^\dagger |0\rangle$, $x = 1, 2, \dots, N$ [20, 45], the following ansatz can be used for the two-polariton

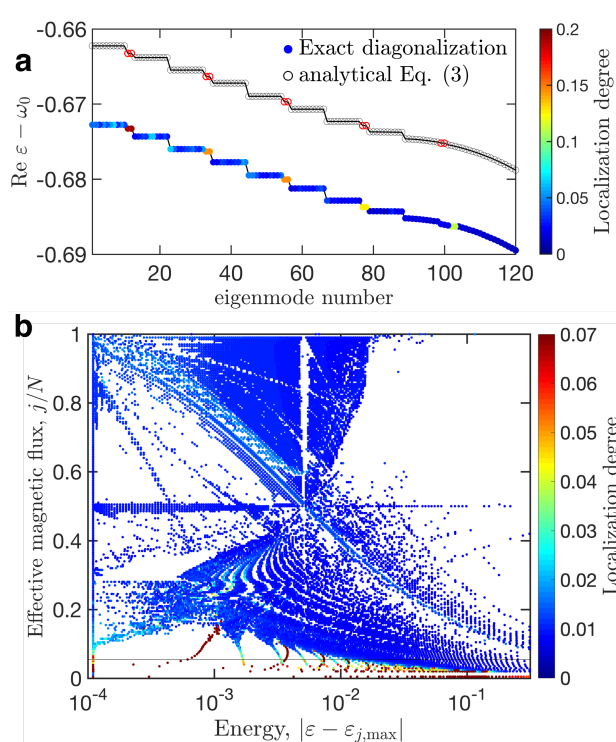


FIG. 3. **Self-induced Hofstadter butterfly.** (a) Energy spectrum for the two-polariton states in the cluster corresponding to $j = 11$, calculated from the approximate Eq. (3) and by the exact diagonalization of the two-particle Hamiltonian Eq. (1). (b) Butterfly energy spectrum obtained by the exact diagonalization as a function of cluster index j , determining the effective magnetic field. Localization degree is determined as the inverse participation ratio of the vector χ in Eq. (2) and is shown by color. Thin horizontal line in (b) indicates magnetic field $j/N = 11/200$, corresponding to panel (a). Calculation has been performed for $N = 200$ and $\varphi = 0.02$, energy is measured in the units of Γ_0 .

state

$$\psi_{xy} = \psi_y^{(j)} \chi_x + \psi_x^{(j)} \chi_y, \quad x, y = 1 \dots N \quad (2)$$

where $\psi_x^{(j)}$ and χ_x are the wave functions of the first and second polaritons. The former is assumed known and corresponds to the standing wave $\psi_x^{(j)} = \cos k_j(x - \frac{1}{2})$. To determine the latter, we derive the Schrödinger equation, that accounts for interaction between the polaritons and reads (see Supplementary Materials for more details)

$$\chi_{x+1} + \chi_{x-1} - 2\chi_x + \left\{ \frac{\omega_0 + \omega_j - 2\varepsilon}{2\varphi\Gamma_0} + \frac{4}{Nk_j^2} \cos^2[k_j(x - \frac{1}{2})] \right\}^{-1} \chi_x = 0, \quad (3)$$

where $\omega_j \approx \omega_0 - 2\varphi\Gamma_0/k_j^2$ is the real part of the eigenfrequency of the single-polaritonic state $\psi^{(j)}$ and $\varphi = \omega_0 d/c$. Equation (3) describes a motion of a particle on a lattice in an external potential of a standing wave with the period N/j . It has a striking similarity to the Harper equation for an electron moving in a square lattice subjected

to the perpendicular magnetic field [46]:

$$\chi_{x+1} + \chi_{x-1} + 2 \cos(2\pi x \alpha - k_y) \chi_x = \varepsilon \chi_x. \quad (4)$$

Here, α is the magnetic flux through the unit cell and k_y is the wave vector in the perpendicular direction. For small magnetic fields $\alpha \ll 1$, the energy spectrum of Eq. (4) is a ladder of degenerate Landau levels for electrons moving along quantized cyclotron orbits. In the finite structure, the edge states of topological nature arise in the gaps between the Landau levels. Such states correspond to electrons moving along skipping orbits at the structure edge, and are the origin for the quantum Hall effect [4].

In our system, the ratio j/N of the cluster index to the total number of atoms in Eq. (3) plays the same role as the magnetic field flux in Eq. (4). The spectrum also consists of degenerate Landau levels and the topological edge states in the gaps between them, see Fig. 3a. The result of exact numerical diagonalization of the two-polariton Hamiltonian Eq. (1) [bold symbols in Fig. 3a] agrees quantitatively with the solution of Eq. (3) [open symbols in Fig. 3a]. Thus, the states Eq. (2) acquire a peculiar internal structure, with nontrivial topology induced by interaction for each of the two indistinguishable polaritons.

The energy spectrum of the Harper Eq. (4) becomes very rich when the magnetic flux α increases. The Landau levels split and transform into a celebrated Hofstadter butterfly [3], shown also in Supplementary Fig. S2. The butterfly has a self-similar structure with q allowed energy bands at the rational fluxes $\alpha = p/q$ [2] and a Cantor-set spectrum for irrational fluxes. Even though in our case the effective magnetic flux j/N is rational, we can still extract an analogue of the Hofstadter butterfly from the two-polariton spectrum in Figs. 2e–g. We separate the clusters in Figs. 2e–h formed by different standing waves (i.e. different effective magnetic fields) and align them horizontally, the details are presented in Methods and Supplementary Fig. S3. The resulting butterfly is shown in Fig. 3b and it qualitatively resembles the Hofstadter butterfly [Fig. S2].

In accordance with Fig. 3a and Fig. 2, for small magnetic fluxes j/N the butterfly in Fig. 3b features distinct Landau levels with edge states in the gaps between them. These edge states correspond to red points in Fig. 3b. At high magnetic fields the Landau levels split, but the spectrum still retains a surprisingly delicate structure.

POLARITON-POLARITON ENTANGLEMENT

The internal structure of the two-polariton states is represented by their entanglement entropy [47], $S = -\sum \lambda_\nu \ln \lambda_\nu$, obtained from the Schmidt expansion $\psi_{nm} = \sum_{\nu=1}^N \sqrt{\lambda_\nu} \psi_n^\nu \psi_m^\nu$, ($\sum \lambda_\nu = 1$). The result, presented in Fig. 4b, demonstrates a rich variety

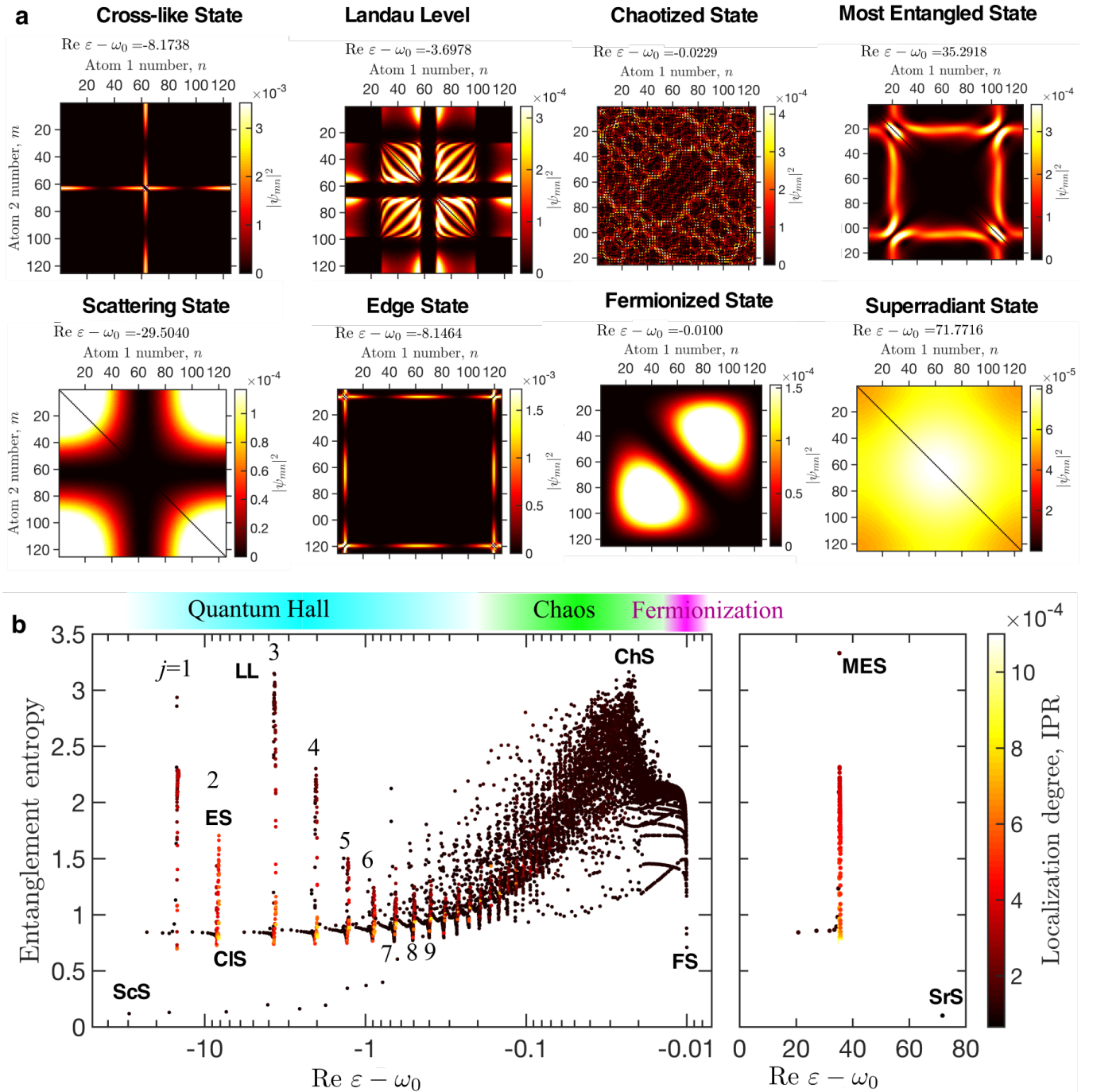


FIG. 4. **Diversity of two-polariton states.** (a) Characteristic wavefunctions for different types of two-polariton states, indicated in (b) by abbreviations. (b) Entanglement entropy depending on the state energy. Color shows the inverse participation ratio that characterizes the localization degree. Left and right panels correspond to the states with $\text{Re } \varepsilon < \omega_0$ and $\text{Re } \varepsilon > \omega_0$, respectively. Standing wave numbers j are indicated near the energy clusters. Calculation has been performed for $N = 125$, $\omega_0 d/c = 0.02$. Energy is measured in the units of Γ_0 .

of eigenstates with different localization degrees, indicated by the color. Characteristic examples of wave functions are shown in Fig. 4a. The entropy of entanglement tells us the number of distinct single-particle states in a given two-body state, so it is low for the scattering states,

where two polaritons are quasi-independent. The topological states Eq. (2) also have an intrinsically low entropy, being just a product of a standing wave and a localized or an edge state. However, the states Eq. (2) can mix with each other resulting in larger entanglement entropy.

This entangled mixing becomes especially prominent for the Landau level states, cf. points LL, CIS and ES in Fig. 4b. When the real part of energy approaches ω_0 from the negative side, the mixing between different standing waves increases since the spectrum gets denser, and the states become chaotic-like, see also the top right corner of Fig. 1d. At very small negative energies $\varepsilon - \omega_0 \sim -\varphi\Gamma_0$ the single-particle dispersion changes from $\varepsilon \propto -1/k^2$ to $\varepsilon \propto -(k - \pi/d)^2$ because both polaritons get closer to the Brillouin zone edge, and the fermionic correlations [26] emerge from chaos. The dense cluster of two-polariton states in the right panel of Fig. 4b, where $\text{Re}\varepsilon > 0$, is formed by the interaction with the quasi-superradiant mode with $\text{Re}\varepsilon - \omega_0 \approx 71\Gamma_0$ in Fig. 2a. It is one of the states of this cluster that has the entanglement entropy even higher than that of the chaotic-like states, see the point MES at $\text{Re}\varepsilon - \omega_0 \approx 35\Gamma_0$.

In summary, we have discovered a novel interaction-induced internal topological order for the two-polariton states in a light-coupled atomic array. We have revealed that the underlying Dicke-type model demonstrates an incredible diversity of quantum states with different topologies, lifetimes, and entanglement in a strikingly simple system. While its importance for quantum optics [22, 23] is already well understood, it could rightfully take its place also in the many-body physics, along with such celebrated examples as a Heisenberg model, Bose-Hubbard model, or a Luttinger liquid. The waveguide-mediated long-ranged couplings are quite uncharacteristic for traditional quantum systems and there is much more to expect. For example, we have focused here only on the regime of extremely subwavelength distances between the atoms, where two-polariton bound states [45, 48] play no role. Polariton-polariton interactions could be even more interesting in the Bragg-spaced lattices, where the non-Markovian effects are drastically enhanced [49–51]. The ultra-strong coupling regime [24] is also unexamined for the quantum waveguides to the best of our knowledge. On the more practical side, it is promising to explore recently proposed high-quality states [52] in the many-body domain to increase the quantum coherence. The waveguide-based setups could be used to route and manipulate signals [53], propagating on future quantum chips [54] and our results open new possibilities to engineer the quantum entanglement.

Author contributions. ANP and AVP conceived the idea and developed an analytical model. JZ, ANP, NAO and YK performed the numerical calculations. ANP, CL, and YSK supervised the project. All authors contributed to discussion of the results and writing the manuscript.

This work was supported by the Australian Research Council. J.Z was supported by Australian Government Research Training Program (RTP) Scholarship. C.L. was supported by the National Natural Science Foundation of China (NNSFC) (grants No. 11874434 and No.

11574405). Y.K. was partially supported by the Office of China Postdoctoral Council (grant No. 20180052), the National Natural Science Foundation of China (grant No. 11904419), and the Australian Research Council (DP200101168). A.V.P. acknowledges a support from the Russian Science Foundation (Project No. 19-72-00080). A.N.P. has been partially supported by the Russian President Grant No. MD-243.2020.2. N.A.O. has been partially supported by the Foundation for the Advancement of Theoretical Physics and Mathematics “BASIS.”

METHODS

Calculation of the energy spectrum of the Hamiltonian Eq. (1), shown in Fig. 2, is relatively straightforward. The spectrum is found by standard linear algebra techniques, see also Supplementary Materials. However, it is more challenging to extract the butterfly spectrum in Fig. 3b from the spectrum in Fig. 2e. This task requires careful separation of the clusters corresponding to different single-polariton states. We start by performing the Schmidt decomposition of the two-polariton state

$$\psi_{xy} = \sum_{\nu=1}^N \sqrt{\lambda_\nu} \psi_x^\nu \psi_y^\nu \quad (\text{M1})$$

for all the states that have $\text{Re}\varepsilon < \omega_0$. Our analysis of the Schmidt decomposition confirms, that for most of the states it is governed by two largest singular values λ_1 and λ_2 , that have close absolute values. Keeping only these two terms, we obtain new linear combinations of the wave functions ψ_x^1 and ψ_y^2 as $u_n^\pm = \lambda_1^{-1/4} \psi_n^1 \pm \lambda_2^{-1/4} \psi_n^2$. After that, the two-polariton state can be approximately presented as $\psi_{xy} \propto u_x^+ u_y^- + u_x^- u_y^+$. Next, we select one of the two states u_x^+ , u_y^- that has lower inverse participation ratio, $\sum |u_x|^4 / [\sum |u_x|^2]^2$, which means it is less localized in space. We designate this state as $u^{(\text{free})}$ and the more localized one as $u^{(\text{loc})}$, perform the discrete Fourier transform

$$u^{(\text{free})}(k) = \sum_{x=1}^N e^{-ikx} u_x^{(\text{free})} \quad (\text{M2})$$

and calculate the wave vector k_{max} , corresponding to the maximum of the Fourier decomposition. The number of the cluster can be then determined from the quantization rule

$$j \approx \left\lceil \frac{k_{\text{max}} N}{\pi} \right\rceil, \quad (\text{M3})$$

where square brackets indicate the rounding to the nearest integer. In order to improve the precision in Eq. (M3) for large j , we also characterize the vectors χ by their mirror symmetry. Then we apply Eq. (M3) separately

for odd and even states with odd and even j , respectively. The results of Fourier transform for $N = 200$ atoms are shown in Figs. S3, S4 of the Supplementary Materials. Except for very large j close to N , the spectrum is clearly separated into well-defined steps of alternating parity. Each step is assigned to a different cluster of eigenvalues. Next, we align the clusters with respect to each other. This is done by subtracting the energy with the largest (smallest negative) real part from the energies of the states of each cluster, $\varepsilon_{j,\max}$. In order to keep the points with the highest energy on the semilogarithmic plot after this subtraction, we also add a small value of $1.1 \times 10^{-4}\Gamma_0$ to all the energies. The result is the butterfly spectrum, shown in Fig. 3b.

* yuri.kivshar@anu.edu.au

† poddubny@coherent.ioffe.ru

- [1] Z. F. Ezawa, *Quantum Hall Effects: Recent Theoretical and Experimental Developments Third Edition* (World Scientific Publishing Company, 2013).
- [2] M. Y. Azbel, “Energy spectrum of a conduction electron in a magnetic field,” *Sov. Phys. JETP* **19**, 634 (1964).
- [3] D. R. Hofstadter, “Energy levels and wave functions of Bloch electrons in rational and irrational magnetic fields,” *Phys. Rev. B* **14**, 2239–2249 (1976).
- [4] D. J. Thouless, M. Kohmoto, M. P. Nightingale, and M. den Nijs, “Quantized Hall conductance in a two-dimensional periodic potential,” *Phys. Rev. Lett.* **49**, 405–408 (1982).
- [5] B. A. Bernevig, T. L. Hughes, and S.-C. Zhang, “Quantum Spin Hall Effect and Topological Phase Transition in HgTe Quantum Wells,” *Science* **314**, 1757–1761 (2006).
- [6] M. Z. Hasan and C. L. Kane, “*Colloquium* : Topological insulators,” *Rev. Mod. Phys.* **82**, 3045–3067 (2010).
- [7] C. R. Dean, L. Wang, P. Maher, C. Forsythe, F. Ghahari, Y. Gao, J. Katoch, M. Ishigami, P. Moon, M. Koshino, T. Taniguchi, K. Watanabe, K. L. Shepard, J. Hone, and P. Kim, “Hofstadter’s butterfly and the fractal quantum Hall effect in moiré superlattices,” *Nature* **497**, 598–602 (2013).
- [8] T. Ozawa, H. M. Price, A. Amo, N. Goldman, M. Hafezi, L. Lu, M. C. Rechtsman, D. Schuster, J. Simon, O. Zeitlinger, and I. Carusotto, “Topological photonics,” *Rev. Mod. Phys.* **91**, 015006 (2019).
- [9] Z. Wang, Y. Chong, J. D. Joannopoulos, and M. Soljačić, “Observation of unidirectional backscattering-immune topological electromagnetic states,” *Nature* **461**, 772–775 (2009).
- [10] F. D. M. Haldane and S. Raghu, “Possible realization of directional optical waveguides in photonic crystals with broken time-reversal symmetry,” *Phys. Rev. Lett.* **100**, 013904 (2008).
- [11] J. Perczel, J. Borregaard, D. E. Chang, S. F. Yelin, and M. D. Lukin, “Topological quantum optics using atomlike emitter arrays coupled to photonic crystals,” *Phys. Rev. Lett.* **124**, 083603 (2020).
- [12] A. B. Khanikaev and G. Shvets, “Two-dimensional topological photonics,” *Nature Photonics* **11**, 763–773 (2017).
- [13] P. Hauke, O. Tieleman, A. Celi, C. Ölschläger, J. Simonet, J. Struck, M. Weinberg, P. Windpassinger, K. Sengstock, M. Lewenstein, and A. Eckardt, “Non-abelian gauge fields and topological insulators in shaken optical lattices,” *Phys. Rev. Lett.* **109**, 145301 (2012).
- [14] D. L. Sounas and A. Alù, “Non-reciprocal photonics based on time modulation,” *Nature Photonics* **11**, 774–783 (2017).
- [15] P. Roushan, C. Neill, J. Tangpanitanon, V. M. Bastidas, A. Megrant, R. Barends, Y. Chen, Z. Chen, B. Chiaro, A. Dunsworth, A. Fowler, B. Foxen, M. Giustina, E. Jeffrey, J. Kelly, E. Lucero, J. Mutus, M. Neeley, C. Quintana, D. Sank, A. Vainsencher, J. Wenner, T. White, H. Neven, D. G. Angelakis, and J. Martinis, “Spectroscopic signatures of localization with interacting photons in superconducting qubits,” *Science* **358**, 1175–1179 (2017).
- [16] A. Dutt, Q. Lin, L. Yuan, M. Minkov, M. Xiao, and S. Fan, “A single photonic cavity with two independent physical synthetic dimensions,” *Science* **367**, 59–64 (2019).
- [17] Y. Hadad, J. C. Soric, A. B. Khanikaev, and A. Alù, “Self-induced topological protection in nonlinear circuit arrays,” *Nature Electronics* **1**, 178–182 (2018).
- [18] D. Smirnova, D. Leykam, Y. Chong, and Y. Kivshar, “Nonlinear topological photonics,” (2019), [arXiv:1912.01784 \[physics.optics\]](https://arxiv.org/abs/1912.01784).
- [19] Y. Ke, A. V. Poshakinskiy, C. Lee, Y. S. Kivshar, and A. N. Poddubny, “Inelastic scattering of photon pairs in qubit arrays with subradiant states,” *Phys. Rev. Lett.* **123**, 253601 (2019).
- [20] J. Zhong, N. A. Olekhno, Y. Ke, A. V. Poshakinskiy, C. Lee, Y. S. Kivshar, and A. N. Poddubny, “Photon-mediated localization in two-level qubit arrays,” *Phys. Rev. Lett.* **124**, 093604 (2020).
- [21] K. M. Birnbaum, A. Boca, R. Miller, A. D. Boozer, T. E. Northup, and H. J. Kimble, “Photon blockade in an optical cavity with one trapped atom,” *Nature (London)* **436**, 87–90 (2005).
- [22] D. Roy, C. M. Wilson, and O. Firstenberg, “*Colloquium*: strongly interacting photons in one-dimensional continuum,” *Rev. Mod. Phys.* **89**, 021001 (2017).
- [23] D. E. Chang, J. S. Douglas, A. González-Tudela, C.-L. Hung, and H. J. Kimble, “*Colloquium*: quantum matter built from nanoscopic lattices of atoms and photons,” *Rev. Mod. Phys.* **90**, 031002 (2018).
- [24] A. F. Kockum, A. Miranowicz, S. D. Liberato, S. Savasta, and F. Nori, “Ultrastrong coupling between light and matter,” *Nature Reviews Physics* **1**, 19–40 (2019).
- [25] R. H. Dicke, “Coherence in Spontaneous Radiation Processes,” *Phys. Rev.* **93**, 99 (1954).
- [26] Y.-X. Zhang and K. Mølmer, “Theory of subradiant states of a one-dimensional two-level atom chain,” *Phys. Rev. Lett.* **122**, 203605 (2019).
- [27] S. Aubry and G. André, “Analyticity breaking and Anderson localization in incommensurate lattices,” *Ann. Isr. Phys. Soc.* **3**, 133 (1980).
- [28] Y. E. Kraus, Y. Lahini, Z. Ringel, M. Verbin, and O. Zeitlinger, “Topological States and Adiabatic Pumping in Quasicrystals,” *Phys. Rev. Lett.* **109**, 106402 (2012).
- [29] A. Poshakinskiy, A. Poddubny, L. Pillozzi, and E. Ivchenko, “Radiative topological states in resonant photonic crystals,” *Phys. Rev. Lett.* **112**, 107403 (2014).

- [30] F. Baboux, E. Levy, A. Lemaître, C. Gómez, E. Galopin, L. Le Gratiet, I. Sagnes, A. Amo, J. Bloch, and E. Akkermans, “Measuring topological invariants from generalized edge states in polaritonic quasicrystals,” *Phys. Rev. B* **95**, 161114 (2017).
- [31] Y. Ke, J. Zhong, A. V. Poshakinskiy, Y. S. Kivshar, A. N. Poddubny, and C. Lee, “Radiative topological biphoton states in modulated qubit arrays,” arXiv e-prints, arXiv:2002.10074 (2020).
- [32] M. Verbin, O. Zilberberg, Y. E. Kraus, Y. Lahini, and Y. Silberberg, “Observation of topological phase transitions in photonic quasicrystals,” *Phys. Rev. Lett.* **110**, 076403 (2013).
- [33] N. V. Corzo, J. Raskop, A. Chandra, A. S. Sheremet, B. Gouraud, and J. Laurat, “Waveguide-coupled single collective excitation of atomic arrays,” *Nature* **566**, 359–362 (2019).
- [34] O. Astafiev, A. M. Zagoskin, A. A. Abdumalikov, Y. A. Pashkin, T. Yamamoto, K. Inomata, Y. Nakamura, and J. S. Tsai, “Resonance fluorescence of a single artificial atom,” *Science* **327**, 840–843 (2010).
- [35] Z. Wang, H. Li, W. Feng, X. Song, C. Song, W. Liu, Q. Guo, X. Zhang, H. Dong, D. Zheng, H. Wang, and D.-W. Wang, “Controllable switching between superradiant and subradiant states in a 10-qubit superconducting circuit,” *Phys. Rev. Lett.* **124**, 013601 (2020).
- [36] S. Haroche, M. Brune, and J. M. Raimond, “From cavity to circuit quantum electrodynamics,” *Nature Physics* **16**, 243–246 (2020).
- [37] A. Browaeys and T. Lahaye, “Many-body physics with individually controlled Rydberg atoms,” *Nature Physics* **16**, 132–142 (2020).
- [38] A. Blais, S. M. Girvin, and W. D. Oliver, “Quantum information processing and quantum optics with circuit quantum electrodynamics,” *Nature Physics* **16**, 247–256 (2020).
- [39] A. A. Clerk, K. W. Lehnert, P. Bertet, J. R. Petta, and Y. Nakamura, “Hybrid quantum systems with circuit quantum electrodynamics,” *Nature Physics* **16**, 257–267 (2020).
- [40] I. Carusotto, A. A. Houck, A. J. Kollár, P. Roushan, D. I. Schuster, and J. Simon, “Photonic materials in circuit quantum electrodynamics,” *Nature Physics* **16**, 268–279 (2020).
- [41] S. Ghosh and T. C. H. Liew, “Quantum computing with exciton-polariton condensates,” *npj Quantum Information* **6** (2020), 10.1038/s41534-020-0244-x.
- [42] A. Albrecht, L. Henriot, A. Asenjo-García, P. B. Dieterle, O. Painter, and D. E. Chang, “Subradiant states of quantum bits coupled to a one-dimensional waveguide,” *New J. Phys.* **21**, 025003 (2019).
- [43] E. L. Ivchenko, “Excitonic polaritons in periodic quantum-well structures,” *Sov. Phys. Sol. State* **33**, 1344–1346 (1991).
- [44] M. R. Vladimirova, E. L. Ivchenko, and A. V. Kavokin, “Exciton polaritons in long-period quantum-well structures,” *Semiconductors* **32**, 90–95 (1998).
- [45] A. N. Poddubny, “Quasi-flat band enables subradiant two-photon bound states,” (2019), arXiv:1912.09197 [quant-ph].
- [46] P. G. Harper, “Single band motion of conduction electrons in a uniform magnetic field,” *Proc. Phys. Soc. Lond. A* **68**, 874 (1955).
- [47] J. Eisert, M. Cramer, and M. B. Plenio, “Colloquium: area laws for the entanglement entropy,” *Rev. Mod. Phys.* **82**, 277–306 (2010).
- [48] Y.-X. Zhang, C. Yu, and K. Mølmer, “Subradiant bound dimer excited states of emitter chains coupled to a one dimensional waveguide,” *Phys. Rev. Research* **2**, 013173 (2020).
- [49] E. L. Ivchenko, A. I. Nesvizhskii, and S. Jorda, “Bragg reflection of light from quantum-well structures,” *Phys. Solid State* **36**, 1156–1161 (1994).
- [50] M. Hübner, J. P. Prineas, C. Ell, P. Brick, E. S. Lee, G. Khitrova, H. M. Gibbs, and S. W. Koch, “Optical Lattices Achieved by Excitons in Periodic Quantum Well Structures,” *Phys. Rev. Lett.* **83**, 2841–2844 (1999).
- [51] D. Goldberg, L. I. Deych, A. A. Lisyansky, Z. Shi, V. M. Menon, V. Tokranov, M. Yakimov, and S. Oktyabrsky, “Exciton-lattice polaritons in multiple-quantum-well-based photonic crystals,” *Nat. Photonics* **3**, 662–666 (2009).
- [52] K. Koshelev, S. Kruk, E. Melik-Gaykazyan, J.-H. Choi, A. Bogdanov, H.-G. Park, and Y. Kivshar, “Subwavelength dielectric resonators for nonlinear nanophotonics,” *Science* **367**, 288–292 (2020).
- [53] P. M. Leung and B. C. Sanders, “Coherent control of microwave pulse storage in superconducting circuits,” *Phys. Rev. Lett.* **109**, 253603 (2012).
- [54] F. Arute, J. M. Martinis, *et al.*, “Quantum supremacy using a programmable superconducting processor,” *Nature* **574**, 505–510 (2019).

Supplementary Materials

CONTENTS

Analytical model for polariton-polariton interactions	9
Fourier analysis of the eigenstates	11

ANALYTICAL MODEL FOR POLARITON-POLARITON INTERACTIONS

In this section, we start from the Hamiltonian (1) in the main text [19, 42]

$$H = \sum_n \omega_0 \sigma_n^\dagger \sigma_n + \sum_{n,m} \sigma_n^\dagger \sigma_m \mathcal{H}_{nm}, \quad (\text{S1})$$

$$\mathcal{H}_{nm} = -i\Gamma_0 e^{i\varphi|n-m|}, \quad \varphi = \frac{\omega_0 d}{c}, \quad (\text{S2})$$

and proceed to derive Eq. (3) that describes an interaction of two polaritons. Substituting the ansatz $|\Psi\rangle = \sum \psi_{mn} \sigma_n^\dagger \sigma_m^\dagger |0\rangle$ into the Schrödinger equation $H\Psi = 2\varepsilon\Psi$ we obtain the two-polariton Schrödinger equation in the form [19, 20]

$$\mathcal{H}_{mn'} \psi_{n'n} + \psi_{mn'} \mathcal{H}_{n'n} - 2\delta_{mn} \mathcal{H}_{nn'} \psi_{n'n} = 2(\varepsilon - \omega_0) \psi_{mn}, \quad (\text{S3})$$

or, in a matrix form,

$$\mathcal{H}\psi + \psi\mathcal{H} - 2 \text{diag}[\text{diag} \mathcal{H}\psi] = 2(\varepsilon - \omega_0)\psi. \quad (\text{S4})$$

Here, the “diag” operator transforms a given matrix to the column-vector filled by the diagonal entries of this matrix, and vice versa.

This system is readily solved numerically after the wavefunction ψ is rewritten in the basis of $N(N-1)/2$ localized states of the type

$$[\tilde{\psi}]_{mn} = [\tilde{\psi}]_{nm} = \frac{1}{\sqrt{2}}, \quad n \neq m.$$

Our next goal is to go beyond Refs. [19, 20, 45] and obtain Eq. (3). To this end, we notice that [20, 45]

$$K \equiv \mathcal{H}^{-1} \approx \frac{1}{2\varphi\Gamma_0} \partial^2, \quad \text{where } \partial^2 \equiv \begin{pmatrix} -1 & 1 & 0 & \dots \\ 1 & -2 & 1 & \dots \\ & & \ddots & \\ \dots & 1 & -2 & 1 \\ \dots & 0 & 1 & -1 \end{pmatrix}. \quad (\text{S5})$$

Here, the matrix ∂^2 represents the one-dimensional discrete Laplacian (or the operator of discrete second-order derivative) This means that for a vector ψ_n with a smooth dependence on n one has

$$[\partial^2 \psi]_n = \psi_{n+1} + \psi_{n-1} - 2\psi_n \approx \frac{d^2 \psi_n}{dn^2}.$$

Thus, for a short-period array with $\varphi \ll 1$ the operator K reduces to the second derivative operator. The inverted Hamiltonian K Eq. (S5) is a sparse matrix with only nearest-neighbor couplings. This fact inspires us to perform the transformation

$$\psi = K\psi'K \quad (\text{S6})$$

that means change of the basis to

$$|x\rangle = \frac{1}{\sqrt{N}} \sum_{n=1}^N e^{i\omega_0 d|x-n|/c} \sigma_n^\dagger |0\rangle, \quad \text{where } x = 1, 2, \dots, N. \quad (\text{S7})$$

This basis inherits the distribution of electric field emitted by a given atom. Indeed, $\exp(i\omega_0 d|x-n|/c)$ is just the photon Green function in one dimension. Since the wave equations for electric field are local, the transformed two-polariton Schrödinger equation will be local as well, i.e. it will involve only sparse matrices. Substituting Eq. (S6) into Eq. (S4) we find [20, 45]

$$K\psi' + \psi'K - 2 \text{diag}[\text{diag} \psi'K] = 2(\varepsilon - \omega_0)K\psi'K. \quad (\text{S8})$$

Next, we look for the solution of the transformed equation (S8) in the form

$$\psi'_{xy} = \psi_y^{(j)} \chi_x + \psi_x^{(j)} \chi_y, \quad x, y = 1 \dots N, \quad (\text{S9})$$

corresponding to Eq. (2) in the main text. Here, one of the two excitations is a single-particle eigenstate of the matrix \mathcal{H} with the eigenfrequency ω_j . Using the definition $K \equiv \mathcal{H}^{-1}$, we find

$$K\psi^{(j)} = \frac{1}{\omega_j} \psi^{(j)}. \quad (\text{S10})$$

The state is normalized as $\sum_x [\psi_x^{(j)}]^2 = 1$. The normalization does not involve complex conjugation, because the original matrix \mathcal{H} is not Hermitian but symmetric. As such, its eigenvectors $\psi^{(j)}$ satisfy the non-conjugated orthogonality condition

$$\langle j|j'\rangle \equiv \sum_{x=1}^N \psi_x^{(j)} \psi_x^{(j')} = \delta_{jj'}. \quad (\text{S11})$$

Due to the translational symmetry the vector $\psi^{(j)}$ is just a standing wave [43]:

$$\psi_x^{(j)} \approx \sqrt{\frac{2}{N}} \cos \frac{\pi j(x-1/2)}{N}. \quad (\text{S12})$$

We note, that the ansatz (S9) and (S12) where the eigenstate $\psi^{(j)}$ does not take into account the interaction effects, works only for the transformed Schrödinger equation (S8). This ansatz does not adequately describe the solutions of the original equation (S4) because the wavefunction ψ' does not turn to zero for $n = m$.

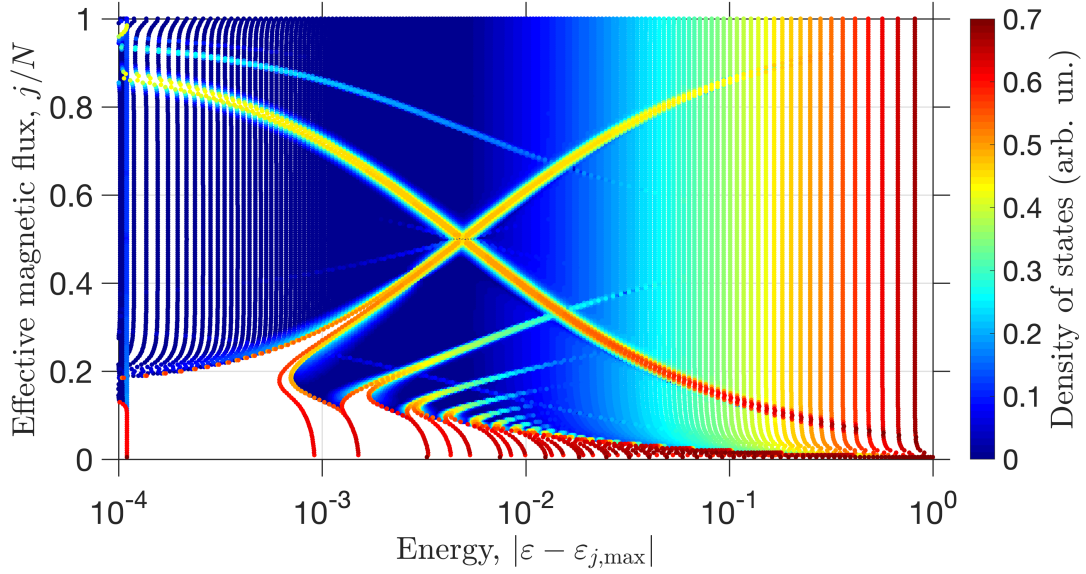


FIG. S1. Butterfly spectrum calculated from Eq. (S17) for $j = 200$, $\varphi = 0.02$. Energy is measured in the units of Γ_0 .

Substituting Eq. (S9) into Eq. (S8), we obtain

$$\begin{aligned} & \frac{\psi_n^{(j)}}{\omega_j} \chi_m + (K\chi)_n \psi_m^{(j)} + \frac{\psi_m^{(j)}}{\omega_j} \chi_n + (K\chi)_m \psi_n^{(j)} \\ & - 2\delta_{mn} \left[\frac{\psi_n^{(j)}}{\omega_j} \chi_n + (K\chi)_n \psi_n^{(j)} \right] \\ & = \frac{2(\varepsilon - \omega_0)}{\omega_j} \left[\psi_n^{(j)} (K\chi)_m + \psi_m^{(j)} (K\chi)_n \right]. \end{aligned} \quad (\text{S13})$$

Next, we multiply this equation by $\psi_m^{(j)}$ and sum over m :

$$\begin{aligned} & \frac{1}{\omega_j} \chi_n + (K\chi)_n + \psi_n^{(j)} \psi_m^{(j)} (K\chi)_m + \frac{\psi_n^{(j)}}{\omega_j} \chi_m \psi_m^{(j)} \\ & - \frac{2}{\omega_j} \psi_n^{(j),2} \chi_n - 2\psi_n^{(j),2} (K\chi)_n \\ & = \frac{2(\varepsilon - \omega_0)}{\omega_j} \left[\psi_n^{(j)} \psi_m^{(j)} (K\chi)_m + (K\chi)_n \right]. \end{aligned} \quad (\text{S14})$$

For the sake of brevity, the summation over the dummy index m is assumed but not indicated explicitly. Using the fact that $\psi^{(j)}$ is the eigenstate of K , we simplify Eq. (S14) to

$$\begin{aligned} & \left[\frac{\chi_n}{\omega_j} + K_{nm} \chi_m + \frac{2}{\omega_j} \psi_n^{(j)} \psi_m^{(j)} \chi_m \right] \\ & - 2\psi_n^{(j),2} \left[\frac{1}{\omega_j} \chi_n + K_{nm} \chi_m \right] \\ & = \frac{2(\varepsilon - \omega_0)}{\omega_j} \left(K_{nm} \chi_m + \frac{1}{\omega_j} \psi_n^{(j)} \psi_m^{(j)} \chi_m \right). \end{aligned} \quad (\text{S15})$$

We are going to consider strongly localized eigenstates that are orthogonal to the standing wave $\psi^{(j)}$. Thus, the

terms $\propto \psi_m^{(j)} \chi_m$ in Eq. (S15) can be omitted to find our main result:

$$\begin{aligned} & \left[\frac{1}{\omega_j} + K \right] \chi - \frac{2}{\omega_j} \text{diag}[\psi^{(j),2}] \chi - \text{diag}[(\psi^{(j),2})K] \chi \\ & = \frac{2(\varepsilon - \omega_0)}{\omega_j} K \chi. \end{aligned} \quad (\text{S16})$$

Moreover, for relatively small j the function χ changes with n much faster than $\psi^{(j)}$. Hence, the term, proportional to $\text{diag}[(\psi^{(j),2})K] \chi$, is larger than the terms $\text{diag}[\psi^{(j),2}] \chi$. Neglecting the terms $\propto \psi_n^{(j),2} \chi_n$, we obtain

$$\left[\frac{1}{\omega_j} + K \right] \chi - 2 \text{diag}[(\psi^{(j),2})K] \chi = \frac{2(\varepsilon - \omega_0)}{\omega_j} K \chi. \quad (\text{S17})$$

Taking Eq. (S5) into account, we get Eq. (3) from the main text, i.e.

$$\begin{aligned} & \chi_{x+1} + \chi_{x-1} - 2\chi_x \\ & + \left\{ \frac{\omega_0 + \omega_j - 2\varepsilon}{2\varphi\Gamma_0} + \frac{4}{Nk_j^2} \cos^2[k_j(x - \frac{1}{2})] \right\}^{-1} \chi_x = 0. \end{aligned} \quad (\text{S18})$$

The butterfly spectrum, calculated from Eq. (S17), is shown in Fig. S1. In the calculation we have neglected the imaginary part of ω_j , replaced the exact operator $K = \mathcal{H}^{-1}$ by its approximation Eq. (S5) and used the analytical expression Eq. (S12) for the wavefunction $\psi^{(j)}$. In order to better resolve the small band gaps at large j we have colored the points by the density of states, with red meaning more dense spectrum. Namely, the color scale corresponds to the logarithm of the fourth derivative of the spectrum ε_ν , $\nu = 1 \dots N$, obtained separately for each value of j . For low j , the result in Fig. S1 is

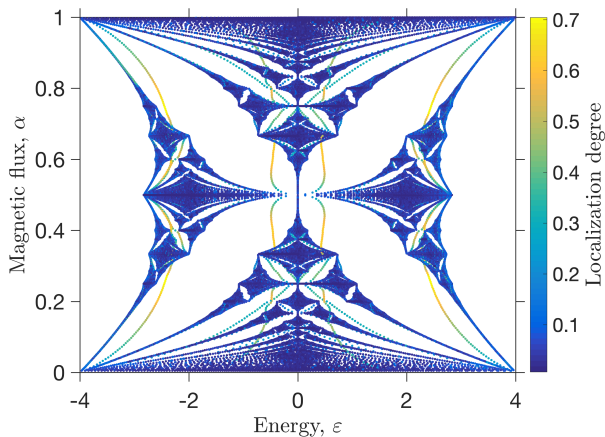


FIG. S2. Hofstadter butterfly obtained from solution of Eq. (S19). Calculation has been performed for an array with $N = 200$ sites, $k_y = 0$, open boundary conditions, and the flux α changing from 0 to 1 with the step $1/(4N)$. Color of the points corresponds to their inverse participation ratio (IPR), higher IPR corresponds to topological edge states.

generally similar to the numerically obtained butterfly, shown in Fig. 3b of the main text. To our surprise, the exact numerical spectrum in Fig. 3b of the main text is actually richer than the semi-analytical one in Fig. S1.

For comparison, we also present in Fig. S2 the original Hofstadter butterfly [3]. It is obtained by studying the dependence of the spectrum of the Harper equation [46] (Eq. (4) in the main text) on the magnetic flux α

$$\chi_{x+1} + \chi_{x-1} + 2 \cos(2\pi x \alpha - k_y) \psi_x = \varepsilon \chi_x. \quad (\text{S19})$$

Three butterfly spectra, calculated from full two-polariton Hamiltonian Eq. (S1), semi-analytical model Eq. (S18) and the Harper equation Eq. (S19), are shown in Fig. S4 (corresponding to Fig. 3b of the main text), Fig. S1 and Fig. S2, respectively. These spectra have both similarities and differences. At low magnetic fields they all demonstrate distinct degenerate Landau levels separated by the band gaps with topological edge states. However, their behavior diverges at higher magnetic fields. The difference between the semi-analytical butterfly in Fig. S1 and the original Hofstadter butterfly in Fig. S2 could be attributed to the peculiar nature of Eq. (S18). Namely, in contrast to the conventional eigenvalue problem Eq. (S19) where the energy ε enters the term in the right-hand side, Eq. (S18) contains the energy ε in the denominator of the last term, i.e. it

is a generalized eigenvalue problem. This is related to the long-ranged photon-mediated couplings between the atoms. Namely, the price for the transformation from the original Hamiltonian Eq. (S3) to the model Eq. (S8) with nearest-neighbor couplings was the appearance of the K operators in the right hand side of Eq. (S8), i.e. the Eq. (S8) became a generalized eigenvalue problem. It is not fully clear at the moment, which of the conclusions derived from the original Harper model Eq. (S19) should be valid for the generalized Aubry-André-Harper model Eq. (3).

As mentioned above, the spectrum of the full Hamiltonian Eq. (S1) is even richer than that of the generalized Aubry-André-Harper model Eq. (3). The reason for this might be the mixing between the standing waves with different orders j that is not accounted in the ansatz Eq. (S12). This mixing becomes prominent for high values of j , as is also indicated by the calculation of the entanglement entropy in Fig. 4 of the main text. It is important, that the butterfly has a fine structure, band gaps and edge states even for high values of effective magnetic flux $j/N \sim 0.3$, see in particular the top state in the left column of Fig. S4.

FOURIER ANALYSIS OF THE EIGENSTATES

We present in Fig. S3 the result of the Fourier analysis of the eigenstates, described in the Methods section of the main text. Figure S4 shows the examples of singular value decomposition for several characteristic two-polariton states.

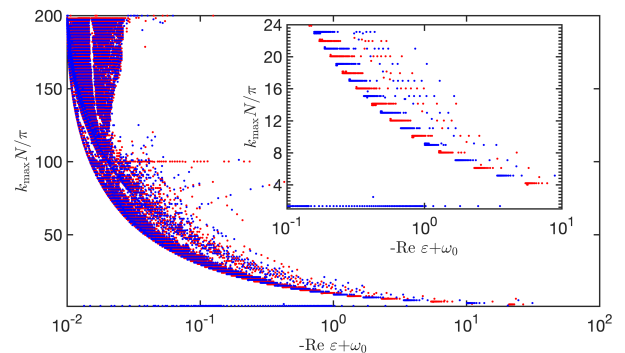


FIG. S3. Fourier analysis of the eigenstates for $N = 200$ atoms, $\varphi = 0.02$. Red and blue colors correspond to even and odd eigenstates, respectively. Inset shows the spectrum in a larger scale for small k_{\max} . Energy is measured in the units of Γ_0 .

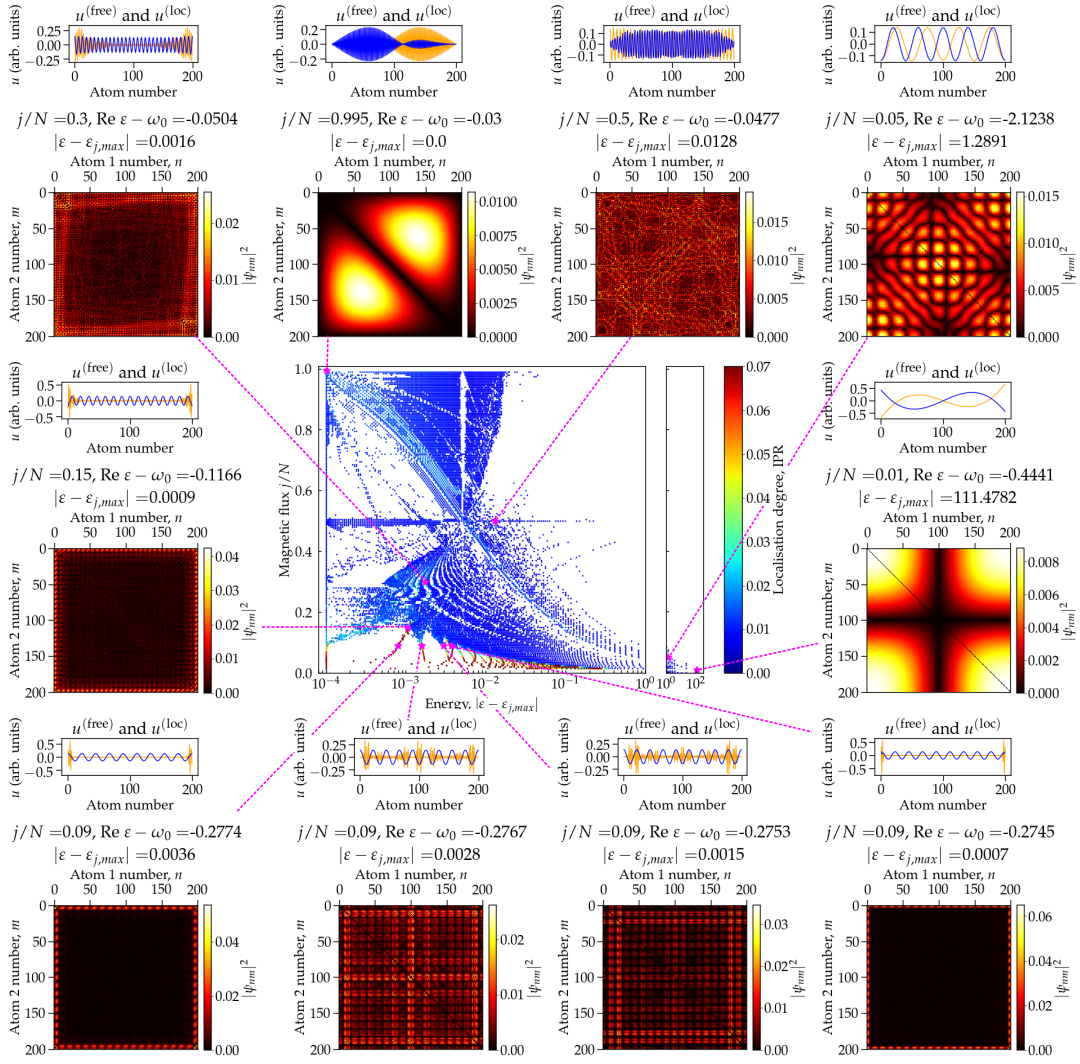


FIG. S4. Butterfly spectrum, corresponding to Fig. 3 from the main text, and several characteristic two-polariton states. For each state we show the whole two-polariton wave function and the real parts of the two vectors $u^{(loc)}$ and $u^{(free)}$, corresponding to leading terms in its singular value decomposition, see Methods. Calculation has been performed for $N = 200$ and $\varphi = 0.02$, energy is measured in the units of Γ_0